ELSEVIER

Surface Science 417 (1998) 361–371

surface science

Structure and morphology of Ni monolayers on W(110)

C. Schmidthals, D. Sander *, A. Enders, J. Kirschner

Max-Planck-Institut für Mikrostrukturphysik, Weinberg 2, D-06120 Halle, Germany

Received 31 March 1998; accepted for publication 3 August 1998

Abstract

Scanning tunneling microscopy (STM) is employed to investigate the structural and morphological properties of Ni monolayers (ML) deposited on W(110) at room temperature. We observe almost perfect layer-by-layer growth for the first three atomic layers. At a coverage of about 6 ML, a transition to three-dimensional growth is found. The analysis of STM images in the submonolayer regime indicates that the coalescence of the islands triggers the formation of a 8×1 coincidence structure. In contrast to the preferential orientation expected from the twofold symmetric substrate, the islands in the first atomic layer have an irregular shape. Elongated Ni islands are observed in the second layer. The anisotropic island shape is ascribed to the anisotropic diffusion due to anisotropic strain in the underlying first layer. The edges of the Ni islands are oriented along the closed packed $\langle 110\rangle$ directions of the growing Ni(111) film for Ni coverages above 5 ML.

Keywords: Morphology; Nickel; Scanning Tunneling Microscopy (STM); Structure; Tungsten

1. Introduction

Growth and morphology of ultrathin ferromagnetic films have attracted much attention recently mainly for two reasons: the reduced dimensionality of such systems gives rise to drastically changed magnetic [1] and elastic [2,3] properties as compared to the respective bulk materials. Potential applications of ultrathin films in storage media led to an increasing interest in ultrathin magnetic films [4]. Due to the close relation between the morphology and the magnetic properties of ultrathin films, as shown for example by investigations of the morphology and the magnetic properties of Fe films on W(110) [5,6], the knowledge of the morphological details is mandatory for an understanding of thin film magnetism.

* Corresponding author. Fax: +49 345 5511 223; e-mail: sander@mpi-halle.de

The goal of this paper is to provide a detailed STM analysis of the structural and morphological properties of Ni monolayers grown on W(110). The structural transitions from pseudomorphic growth over coincidence structures finally to a fcc(111)-like Ni film, which grows in the Nishiyama–Wassermann orientation [7] on W(110), are discussed. Some contradictions found in the literature concerning the growth mode are clarified in this work.

Layer-by-layer growth up to 2 ML at room temperature followed by a transition to three-dimensional growth was discussed in the early work of Kolaczkiewicz and Bauer [7]. Using low-energy electron diffraction (LEED), several changes of the diffraction patterns were observed with increasing coverage in the submonolayer range, indicating transitions from a pseudomorphic state to a 8×1 coincidence structure and

0039-6028/98/$ – see front matter
PII: S0039-6028(98)00689-X

another transition to a 7×1 coincidence structure. In contrast, a later LEED study [8] suggested pseudomorphic growth up to one monolayer. Layer-by-layer growth up to 3 ML [9] was reported by depositon at elevated temperatures, obtained by the analysis of intensity changes versus coverage in Auger electron spectroscopy experiments. Layer-by-layer growth up to 5 ML was proposed, based on the observation of intensity oscillations in reflection high energy diffraction experiments [10] for deposition at room temperature, whereas deposition at low temperatures led to the conclusion of layer-by-layer growth for up to 40 layers [10]. Employing high-energy ion backscattering [11], double-layer growth was proposed in the submonolayer range.

In this paper, we present an STM investigation of the morphology of ultrathin Ni films on W(110) grown at room temperature, providing the first real space data of the growth in this system. We observe almost perfect layer-by-layer growth for the first three layers. Starting at a coverage of about 6 ML, a gradual transition to three-dimensional growth is observed. A double-layer growth mode in the submonolayer range cannot be confirmed. Annealing the films leads to the formation of three-dimensional islands on top of one stable atomic layer, indicating Stranski–Krastanov growth in thermal equilibrium.

A careful analysis of the apparent coverage as calculated from STM images gives direct evidence for the changes of the areal atomic density in the growing film. The analysis of STM images in the submonolayer regime indicates that the coalescence of the islands triggers the formation of the 8×1 coincidence structure. In contrast to Cu on W(110) [12], the first atomic layer retains its initial structure upon further Ni deposition. The elongated island shapes observed for growth of the second layer are ascribed to the strain state of the growing film.

2. Experimental

A detailed description of the experimental setup has been published elsewhere [13], and we restrict ourselves to a short survey of the experimental procedures employed. The results presented in this article were obtained under ultra-high-vacuum conditions with a base pressure of 6×10^{-11} mbar. The chamber was equipped with a custom-designed STM [14] and a cylindrical mirror analyser (CMA)-based Auger system for checking the sample cleanliness. Structural information obtained by a commercial Spot Profile Analizing LEED system (SPA-LEED) (Typ NG-SPA, Version 1.2, Omicron Vakuumphysik GmbH, Taunusstein, Germany, based on a development, described in Ref. [15]), mounted in the same chamber, has been presented elsewhere [13]. Ni films were deposited on the substrate at room temperature by thermal sublimation of an ultraclean (99.999%) Nickel rod, heated by electron bombardment with growth rates of about 0.5 ML min^{-1}. The pressure during deposition never rose above 5×10^{-10} mbar. The amount of deposited Ni has been controlled with a quartz microbalance. The microbalance was calibrated by refering to our STM coverage analysis at higher Ni coverages. We estimate an upper limit for the error of the amount of deposited Ni of $\pm 10\%$.

For STM investigations, the Ni coverage was incrementally increased by small deposits of about 0.2 ML. During deposition, the STM tip was fully retracted by 1 μm from the sample surface by applying the maximum piezo voltage. After each deposition step, the same surface area could be retrieved allowing the investigation of the film growth at the same surface position over the whole thinkness range of interest. Coverage calibration was accomplished by imaging the surface after each evaporation step and calculating the distribution of Ni in all monoatomic layers. We estimate the accuracy of this calibration to be better than 0.1 atomic layers (AL). AL represent the fraction of the substrate area covered by Ni. Therefore, depending on the density of the growing film, coverages stated in units of AL (denoted apparent coverage) might be different to those stated in units of monolayers (ML), which, in this paper, are given by the packing density of the fcc Ni (111) plane of bulk Ni ($1\ \mathrm{ML} = 1.86 \times 10^{15}$ atoms cm^{-2}). The connection between the apparent coverage given in units of

AL and the deposited amount of Ni given in ML is discussed in detail below.

3. Results and discussion

3.1. Structure of ultrathin Ni films on W(110)

Our results indicate, that the morphology of Ni monolayers depends strongly on the strains in the growing film. Therefore, we begin with a discussion of the film structure before we present our results on the morphology of Ni monolayers.

Since our results on the Ni film structure are in full agreement with previous studies [7] and have already been described by us [13,16], only a short survey is given. The results are summarized in Table 1.

In the monolayer range, the film structure undergoes an evolution through three distinctly different configurations with increasing coverage: up to 0.2 ML, the islands are pseudomorphic to the substrate, as deduced from the 1×1 diffraction pattern with no notable increase in background intensity. In the Nishiyama–Wassermann orientation [7], which we observe above 1 ML, the Ni(111) plane lies parallel to the W(110) plane and the Ni$\langle 0\bar{1}1 \rangle$ directions are parallel to the W$\langle 001 \rangle$ directions. Assuming this epitaxial orientation for coverages below 0.2 ML a strongly anisotropic strain [3] in the pseudomorphic phase of enormous 27% along the W[001] direction and moderate 3.7% in the W[1$\bar{1}$0] direction builds up, assuming the respective Ni–Ni distances in bulk Ni(111) as a reference and neglecting possible relaxations. Above 0.2 ML, the strain energy is lowered by forming a 8×1 coincidence structure, where 9 Ni–Ni atomic distances correspond to 8 W–W atomic distances. In this configuration, the tensile strain in the Ni film is reduced from 27% to 13% in the W[001] direction. A configuration where 10 Ni–Ni distances equal 8 W–W distances reduces the strain of the 8×1 coincidence structure even further to 1.6%. From our LEED, STM, and stress measurements [3,16], we cannot decide which configuration resembles the 8×1 coincidence structure. Strain and areal density data for both configurations are given in Table 1. Further Ni deposition leads to the formation of a 7×1 coincidence structure, starting at a coverage of

Table 1
Summary of the structural evolution with increasing coverage

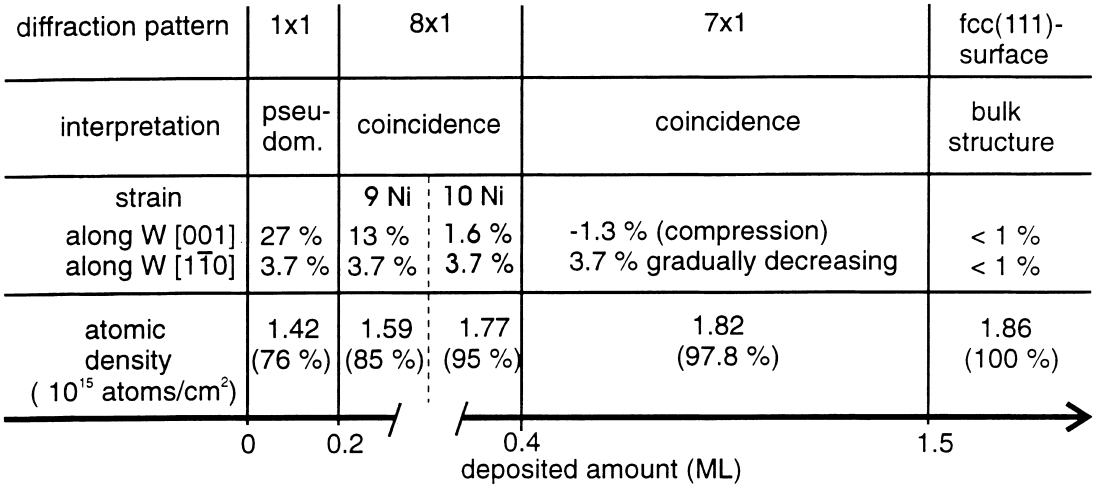

The observed LEED pattern are stated together with the interpretation, the resulting strain in the film and the packing density, calculated for an ideal film in the respective strain state. Numbers in brackets represent the percentage of the density of the (111) plane of bulk Ni. The strains are calculated, using the atomic distances in the (111) plane of bulk Ni as a reference. For the 8×1 structure, data for configurations with nine Ni atoms and with 10 Ni atoms are given (see Section 3.1)

0.4 ML. Here, every tenth Ni atom coincides with every eighth W atom, thus leading to a correspondence of 9 Ni–Ni atomic distances to 7 W–W atomic distances. In this configuration, the strain in W[001] direction is further reduced to a slight compression of −1.3%. In diffraction experiments with conventional LEED optics, no shift in the diffraction spots in W[1$\bar{1}$0] direction could be observed within the limit of accuracy of about 2%. Despite the increased angular resolution of our SPA-LEED instrument, again an accuracy of only 2% is obtained, due to deviations from a linear voltage–distance behaviour when scanning large distances in reciprocal space. Therefore, we conclude that the film retains its strain of 3.7% in the W[1$\bar{1}$0] direction, when the first monolayer is completed. The 7×1 coincidence structure leads to a corrugation of the surface, which can be seen in STM images as periodic arrangement of stripes along the W[001] direction [13].

As indicated in Table 1, the 7×1 coincidence structure has almost the same atomic density as the dense fcc(111) plane and resembles a slightly distorted fcc(111) unit cell. The reduction of the strain energy and the increase of the in-plane coordination seem to be important factors for the formation of the 7×1 structure. Consequently, further deposition of Ni leads to the growth of a slightly distorted fcc(111) oriented film with some residual strain, as evidenced by direct measurements of the film stress [3].

Additional insight into the structural evolution from a pseudomorphic phase to the formation of a fcc(111)-like Ni film is obtained by the analysis of STM images. In Fig. 1, we plot the apparent coverage, as obtained from calculating the fractional coverage of the substrate by Ni from STM images in AL, as a function of the deposited amount of material. Fig. 1 clearly indicates that the curve consists of line segments with varying slopes. Each line segment has been assigned to a coverage range, denoted I to V in Fig. 1, and is characterized by distinct structural phases, as obtained by LEED and STM. The slope of each segment is reciprocally proportional to the packing densitiy of the growing film. For example, in region II, more material has to be deposited to increase the apparent coverage as seen on STM images,

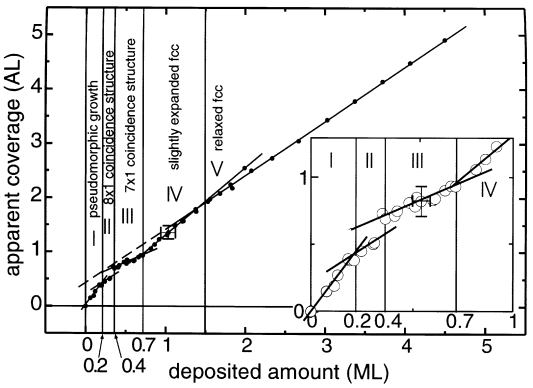

Fig. 1. Apparent coverage as calculated from STM images as a function of deposited amount of material. Different slopes correspond to different atomic densities of the growing film. The range up to 1 ML is shown in an inset for better illustration. Each line segment can be attributed to a certain structural configuration, the coverage ranges being denoted region I to V. (1 ML Ni = 1.86×10^{15} atoms cm^{-2})

than in region I. This leads to the conclusion, that the packing density is higher between 0.2 and 0.4 ML than below this coverage, indicating the structural transition from the loosely packed pseudomorphic configuration with a packing density of only 1.42×10^{15} atoms cm^{-2} (Table 1) to the more densely packed 8×1 coincidence structure. The packing densitiy is further increased in the range between 0.4 and 0.7 ML, reflecting the increased density of the 7×1 structure in region III. The remaining pseudomorphic patches on the surface, as deduced from STM images [13], only lead to a minor deviation from the density of the 7×1 structure of a few per cent. The densitiy of the deposited material in the second atomic layer is smaller than in the 7×1 structure, as indicated by the increased slope of the curve above 0.7 ML in region IV. LEED experiments reveal an undistorted, but strained fcc(111) pattern for coverages above 0.7 ML. We conclude that in the second atomic layer, the atoms are situated at positions corresponding to an undistorted, but slightly expanded fcc(111) lattice. Tensile film stress in this coverage range [3,16] corroborates this interpretation. The change in slope of the apparent coverage curve at 1.5 ML marks the completion of the second atomic layer, leading to a higher packing density above this coverage in region V.

For higher coverages up to 10 ML, no further slope changes were observed. Measurements of a small tensile film stress [16] in this coverage range indicate that the films are slightly expanded, which can be explained by some residual strain like in other heteroepitaxial systems [17]. Note that in Fig. 1, the slopes of the line segments in the range, where the coincidence structures are observed (region II and III between 0.2 and 0.7 ML), are too small as compared to the slope of the almost relaxed film. We propose that for every incremental increase in coverage, not only are the additional atoms adsorbed in the more densely packed coincidence structures, but also pseudomorphic areas transform into coincidence structures. Thus, the apparent coverage increases more slowly per deposited amount than without the transformation of the pseudomorphic areas. This leads to a smaller slope of the apparent coverage in Fig. 1. Fig. 1 shows a continuous curve that connects different structural regimes. Only at the 7×1 structure the apparent coverage changes with a step. We discuss the slope changes at points, where the curve is continuous first, followed by a discussion of the step in the curve of Fig. 1 at 0.4 ML.

A continuous curve of the apparent coverage vs deposited amount of film material can be interpreted in two ways: (1) only the additionally adsorbed atoms have an arrangement with a different density, whereas the already existing layers and islands keep their density; or (2) with each increment in coverage, a fixed fraction of the already existing islands transform into the newly developing structural phase. Because for the 8×1 and the 7×1 structure our measurements give a slope that is too small (with the densities being too high), interpretation (1) seems more likely for these configurations, though we cannot provide any direct experimental evidence for this mechanism. The slope changes at 0.7 and 1.5 ML, where a continuous curve is observed, take place just when an atomic layer is completed (at 1 and 2 AL, respectively). Thermal desorption experiments [8] and calculations [18] have shown that the bond strength decreases from the first to the second and from second to the third atomic layer. Therefore, the observed density changes at 0.7 and 1.5 ML are more likely restricted to the newly forming atomic layer and do not affect the layer underneath, as the Ni in the underlying layers is stronger bonded to the substrate than the additional layers are. Thus, for these transitions, which occur at the completion of an atomic layer, interpretation (1) seems to be more likely, though again we cannot present a direct experimental proof for this mechanism. The step at the transition from the 8×1 to the 7×1 structure cannot simply be intepreted as a transformation of all the 8×1 patches because this would lead to a jump to a smaller apparent coverage in contrast to the observed step upwards. Obviously, parts of the already existing islands transform into a much more loosely packed arrangement. A partial transformation of the 7×1 phase to the pseudomorphic configuration with its lower atomic density (Table 1) would be a plausible explanation. However, we can only speculate on this possiblility because we did not achieve atomic resolution with our STM. Therefore, the observed step of the packing density at the transition from the 8×1 to the 7×1 still remains to be investigated.

Note that the curve for coverages above 1.5 ML does not intersect the apparent coverage axis at the origin, as indicated by the extrapolated broken line. Furthermore, above 1.5 ML, no slope changes have been observed, suggesting that the packing density in the third and higher atomic layer as well as the density in the first two layers do not change upon further deposition. We conclude, therefore, that the areal density of thicker films varies in the direction normal to the film surface. This behaviour is in contrast to the growth of Cu on W(110), where the initially pseudomorphic first monolayers rearrange upon further deposition, so that the most densely packed rows of the film and the substrate coincide (Kurdjumov–Sachs orientation) [12].

3.2. *Morphology of ultrathin Ni films on W(110)*

In the following discussion of film morphology, the consideration of the strain state is of considerable importance for the discussion of the island shapes.

In Fig. 2, a series of STM images of the same surface area with film coverages from 0.4 AL up

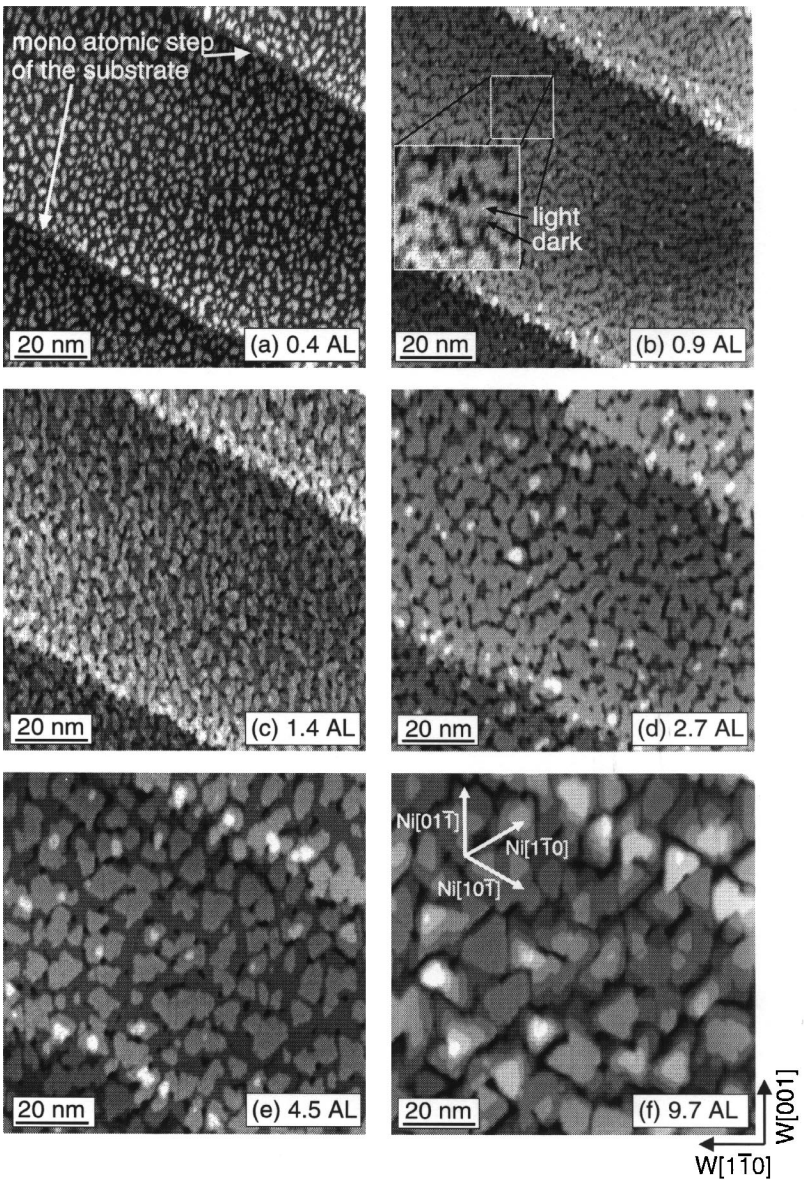

Fig. 2. STM images of the same surface region for different Ni coverages on W(110), $T_{ad} = 300$ K. Stripes from the upper left to the lower right corner represent monatomic steps of the substrate. (a) 0.4 AL. Irregular-shaped islands with no clear preferential orientation are observed as grey patches on the black substrate. (b) 0.9 AL. A few holes (black) in the almost closed first AL (grey) can be seen. Darker and lighter grey patches within the first layer are marked by arrows, indicating pseudomorphic (darker) areas and those with a 7×1 coincidence structure. (c) 1.4 AL. In the second AL (light grey), the islands show a clear preferential orientation along W[001]. The first layer (dark grey) is not completely closed, and several holes (black) are visible. (d) 2.7 AL. The second AL (dark grey) is almost filled, whereas the third layer (light grey) is filled by 70%. Only very few islands in the fourth layer are present, indicating almost perfect layer-by-layer growth at this coverage. (e) 4.5 AL. Some black holes in the fourth layer can be seen. Although the fifth layer is filled by only 50%, some islands in the sixth layer (white) can be observed, indicating the beginning of three-dimensional growth. The islands edges show a slight preferential orientation, which is seen more clearly at higher coverages. (f) 9.7 AL. The islands show a preferential orientation along the $\langle 110 \rangle$ directions of the growing Ni(111) film. At this coverage, 7 AL are visible on the surface, indicating three-dimensional growth.

to almost 10 AL is shown to indicate the pronounced changes of the film morphology with increasing coverage.

In Fig. 2a, an STM image of a film with a coverage of 0.4 AL is displayed. In this and in all subsequent STM images, the stripes in the upper right and the lower left corner are monoatomic steps of the substrate. Islands in the first Ni layer appear light grey in Fig. 2a, whereas the darker grey patches represent the substrate. Fig. 2a clearly indicates that in the submonolayer coverage range, the islands have irregular shapes without a clear preferential orientation. The missing preferential orientation of the islands seems surprising because of the twofold symmetry of the W(110) surface and because anisotropic diffusion has been observed on a macroscopic scale [19]. As discussed above, in this coverage range, the film grows pseudomorphically on the substrate, leading to anisotropic strain, which differs by a factor larger than 7 (Table 1). If only strain arguments are taken into account, an expansion of Ni islands along the W[001] direction costs 50 times more strain energy than expanded growth along W [1$\bar{1}$0]. Thus, the anisotropic strain in the pseudomorphic coverage range should strongly favour anisotropic island shapes. However, measurements of the film stress [3,16] in this coverage range show compressive stress, in sharp contrast to the predicted tensile stress based on strain arguments. This indicates that strain arguments have a diminished importance in the submonolayer range. The apparent discrepancy between the presumed strain state and measured film stress is resolved when the special electronic properties of small Ni islands on W are taken into account. As photoemission experiments [20–22] have revealed, the strong interaction between Ni and W leads to a strongly modified electronic structure of Ni monolayers on W(110). Assuming that the Ni–Ni bonds are predominantly due to electrons from Ni 3d and 4s bands [23], it seems questionable whether Ni bulk atomic distances should be taken as a reference in the absence of a Ni bulk like electronic d-band. We conclude, therefore, that at least in the submonolayer range below about 0.4 AL, strain arguments based on bulk atomic Ni–Ni distances are of minor importance and that the stress behaviour has to be ascribed to the surface stress of the Ni–W composite.

In order to obtain information on the nucleation and the coalescence of islands in the first atomic layer, the island density is plotted as a function of the coverage in units of AL in Fig. 3. Up to a coverage of about 0.4 AL, the island density increases with coverage, indicating that in this coverage range, nucleation is the dominant growth process. The decrease of the island density for higher coverages above 0.4 AL indicates the coalescence of the islands. As shown above, the formation of the 8×1 coincidence structure also takes place at about 0.4 AL. We conclude that the formation of the 8×1 structure is triggered by the coalescence of the islands. For geometrical reasons, it is evident that the ratio of the number of island edge atoms to the number of atoms in the interior of the island increases with decreasing island size. Assuming that edge atoms can relax inwardly to the relief part of their strain energy as proposed to explain observations obtained in diffraction experiments [24], the formation of many small islands seems more favourable than the growth of a few large islands for a given coverage. Consequently, when the islands become larger than a critical island size, the strain relief by the formation of the 8×1 coincidence structure is more effective than the inward relaxation of edge atoms

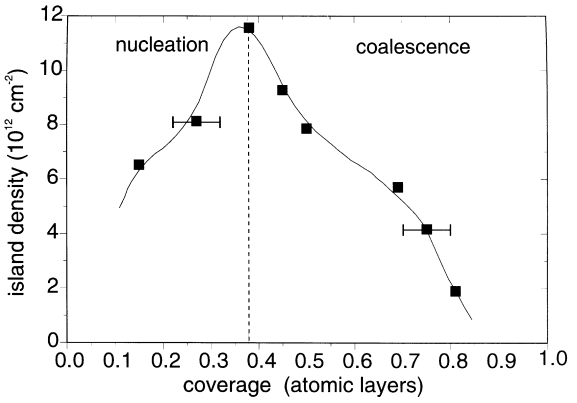

Fig. 3. Island density for the growth of a Ni film in the submonolayer coverage range. The increase between 0 and 0.4 AL indicates nucleation of islands. The decrease above 0.4 AL is attributed to the coalescence of the islands. The line serves as guide to the eye.

as the ratio of edge atoms to inner atoms decreases for larger island sizes. The relaxation of edge atoms has also been discussed to explain the hindered coalescence of Fe islands on W(110) [25]. Note that at a coverage of 0.4 AL, the average Ni island diameter is about 2 nm, corresponding to six W atom diameters along the W[001] direction. Since the unit cell of the 8×1 coincidence structure has a size of at least eight atomic spacings along the W[001] direction, an island size of at least 2.5 nm, as obtained by the coalescence, seems to be necessary for the formation of this structure. Therefore, our STM investigation presents clear evidence that the coalescence of the islands triggers the formation of the 8×1 coincidence structure, as has been conjectured in an early LEED study [7].

At a coverage of 0.9 AL, Fig. 2b reveals that only very few nuclei can be found in the second Ni layer (white spots), indicating layer-by-layer growth in this coverage range. Within the almost closed first layer of Ni (grey), several holes down to the substrate (black) are still visible. However, even within the first Ni layer, a slight contrast represented by darker and lighter grey patches is recognizable, as indicated in the inset of Fig. 2b. This contrast results from the different structure of the film in adjacent areas: dark areas are ascribed to pseudomorphic areas, whereas lighter patches have a 7×1 coincidence structure. The area covered by the 7×1 coincidence structure amounts to about 90% of surface. We have discussed the coexistence of different structural phases in the Ni film on W(110) previously [13].

When the coverage is further increased to 1.4 AL, as shown in Fig. 2c, islands with a distinct preferential orientation along the W[001] direction form on the terraces. At this coverage, the first layer is not yet completely closed, as indicated by the holes (black) in the first Ni layer (dark grey). The islands in the second layer (light grey) show a varying length in W[001] direction, but are clearly longer in that direction than along W $[1\bar{1}0]$. This orientation can be ascribed to the strain state of the underlying first layer (-1.3% along the W[001] direction, 3.7% along the W $[1\bar{1}0]$ direction). As stated above, in the second atomic layer, the islands are strained isotropically. Therefore, the strains in the second atomic layer cannot explain the observed anisotropy of the island shape. As has been shown previously [13], the atomic arrangement in the first Ni layer leads to a wavy surface with channels along the W $[1\bar{1}0]$ direction. The diffusion could be influenced by this corrugation as observed for the channel structure of the Ni(110) surface [26,27]. In that example, a preferential diffusion along the channels was observed and would lead to a preferential diffusion along W$[1\bar{1}0]$, resulting in an extended island length along W$[1\bar{1}0]$. This, however, is in contrast to the observed orientation of the islands, which we explain by the much smaller amplitude of the corrugation caused by the 7×1 coincidence structure compared to the channel depth on the Ni(110) surface. Monte Carlo simulations for the system Fe on W(110) [28] have shown that the observed elongation in W[001] can only be explained by including a different bond strength in the W[001] and W$[1\bar{1}0]$ direction. For Fe/W(110), the interaction of the adsorbed atoms with the nearest neighbors in one direction and next-nearest neighbors in the other direction leads to anisotropic adsorption and diffusion probabilities along the island edges. Recent ab-initio calculations of the hopping diffusion of Al on Al(111) [29] have revealed that the energy barriers for surface diffusion strongly depend on the strain state of the underlying film. The calculations predict that tensile strain leads to higher diffusion barriers, whereas compressive strain results in a decrease in diffusion barriers. As mentioned above, most of the first atomic Ni layer shows compressive strain in W[001] and tensile strain in the W$[1\bar{1}0]$ direction. Therefore, the barrier for diffusion is expected to be smaller along W[001] than in the W$[1\bar{1}0]$ direction, based on the strain dependence of the diffusion barriers [29]. This anisotropy of the diffusion barriers could explain the occurence of islands, which are elongated along W[001].

When the coverage is further increased, the islands in the third layer show no preferential orientation. The film continues to grow in an almost perfect layer-by-layer growth mode. This is demonstrated for a film with a coverage of 2.7 AL in Fig. 2d. At this coverage, the second layer (dark grey) is filled by 98% with some holes down to the

first layer (black), whereas the third layer (light grey) contains about 70% of an AL. The few islands in the fourth layer (white) amout to only 3% of an AL.

At even higher coverages, the islands edges gradually run along a preferential orientation. This is demonstrated in Fig. 2e, showing an STM image of a film with a coverage of 4.5 AL. Since the Ni film on W(110) grows in the Nishijama–Wassermann orientation [7], the preferential orientations of the island edges can be identified as the ⟨110⟩ directions of the growing film. Although the fifth layer (light grey) is only half filled, some small islands have already formed in the sixth layer (white). With increasing film thickness, a gradual transition to three-dimensional growth is observed, as evidenced by an STM image of a film with a coverage of 9.7 AL in Fig. 2f. Here, seven layers are visible, clearly indicating three-dimensional growth in this coverage range. The preferential orientation of the island edges is easily recognized. The islands roughly display a hexagonal shape with the island edges oriented parallel to the ⟨110⟩ directions of the Ni film. STM investigations of the homoepitaxial growth of Pt on Pt(111) [30] have shown that for this surface, having the same symmetry as our Ni(111) oriented films, hexagonally shaped islands are also observed. The exact island shape for the case of Pt was found to be dependent on the growth temperature. This result has been confirmed by dynamic Monte Carlo simulations [31], explaining the observed temperature-dependent shapes by the inequality of the island step microfacets in the closed packed directions of the substrate. A similar behaviour was also predicted for the growth of Al on Al(111) by total energy calculations employing density functional theory [32]. For this case, a hexagonal island shape was predicted in thermal equilibrium for deposition at slightly elevated temperatures above 320 K. In analogy to these examples, we conclude that for the growth of Ni on W(110) above coverages of 5 ML, the hexagonal shape of the islands reflects the sixfold in-plane symmetry of the Ni(111) film, which grows in the Nishiyama–Wassermann orientation on the W substrate. Since we only deposited Ni films at room temperature, we cannot give experimental proof that the observed island shapes correspond to the equilibrium shape or are determined mainly by growth kinetics. Unfortunately, to our knowledge, no experimental investigation of the growth of Ni on Ni(111) has been published so far; thus, comparison with the homoepitaxial growth of Ni is not possible.

The transition from an initial layer-by-layer growth mode to three-dimensional growth is obvious from an analysis of the partial fillings of each layer as a function of coverage in Fig. 4. Broken lines have been added for the first seven layers to represent perfect layer-by-layer growth. From Fig. 4, it is evident that perfect two-dimensional growth is almost fulfilled by the first three layers, whereas the decreasing slope of the curves for higher coverages indicates a gradual transition to three-dimensional growth. The plot shows that the partial coverage of layer $(n-1)$, at which the layer n just starts to grow, decreases from 0.9 AL for the first layer to 0.1 AL for the tenth layer. The aquisition of the STM images of the above discussed series up to about 10 AL lasted for 15 h because one STM image was recorded between each deposition step of 0.2 ML. Nevertheless, the long aquisition time has no influence on the morphology of the films. This was confirmed by deposition of a 10 AL film within 1 h, which showed qualitatively the same morphology as the film deposited in 15 h. The plot in Fig. 4 indicates that

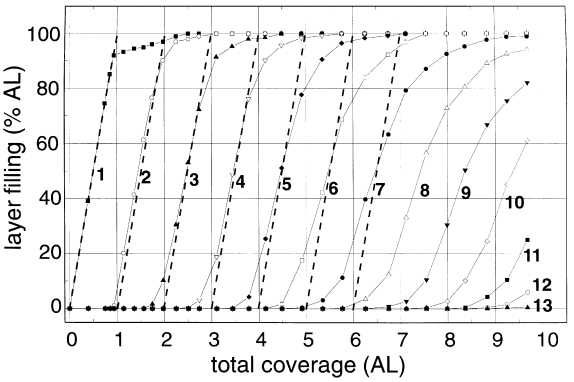

Fig. 4. Layer filling for the growth of a Ni film as a function of the total coverage. The decreasing slope starting at a total coverage of about 3 AL indicates the transition to three-dimensional growth. For perfect layer-by-layer growth, the curves should follow the broken lines.

Ni films on W(110) grow layer-by-layer for coverages up to 6 AL, corresponding to a deposition of 5.6 ML Ni. The transition from layer-by-layer growth to three-dimensional growth in the coverage range of 3–6 ML is in contrast to previous work that described layer-by-layer growth only up to 2 ML [7]. We cannot confirm a double-layer growth mode suggested by results obtained from ion-scattering experiments [11]. In those experiments, it was suggested that the growth of Ni on W(110) is very sensitive to the growth conditions, leading to the observed double-layer growth mode. The fact, however, that the same morphology is observed for films deposited in 15 h and within 1 h indicates that the growth behaviour is not very sensitive to the preparation conditions. Layer-by-layer growth up to 30 ML [33] cannot be confirmed either. In Ref. [33], no statement about the growth temperature was given since, for lower temperatures, up to 40 intensity oscillations in diffraction experiments [10] indicate layer-by-layer growth at 100 K up to 40 ML. At 300 K, however, only up to five oscillations have been observed [10], in good agreement with our results.

In order to obtain additional information on the equilibrium growth mode, we annealed the films. For films with submonolayer coverages, STM images revealed that the first atomic layer was stable at 900 K, and no island formation could be observed. Additionally, no significant changes in the LEED pattern were obtained. An example of an annealed film with higher coverage can be seen in Fig. 5a. Here, a total amount of 1.9 AL Ni was deposited. After deposition at 300 K the film was annealed to 790 K for several minutes. The stripes from the upper left corner to the lower right corner represent steps of the substrate. Several three-dimensional islands can be seen on the surface with locally varying heights, appearing white in Fig. 5a. Because the first atomic layer is stable at 900 K, the regions between the islands are ascribed to a Ni monolayer, as confirmed by Auger electron microscopy [19]. The edges of the three-dimensional islands are roughly oriented along the ⟨110⟩ direction of the Ni film, which reflects the sixfold in-plane symmetry of the fcc(111) surface. However, the island shape could be greatly influenced by the substrate steps, which has been shown using Auger electron microscopy [19]. The locally varying thickness of the wedge shaped islands is shown in Fig. 5b, whith data obtained from a line scan along the line in Fig. 5a. For a better illustration, a schematic drawing of the substrate steps has been added in Fig. 5b. The line scan indicates that the islands have locally varying heights beween 3 and 5 AL, due to the substrate steps in this region. We conclude, that upon annealing, three-dimensional islands form on top of a stable first atomic layer. This temperature-driven morphological transition suggests that under equilibrium conditions, the growth of Ni on W(110) proceeds in the Stranski–Krastanov growth mode.

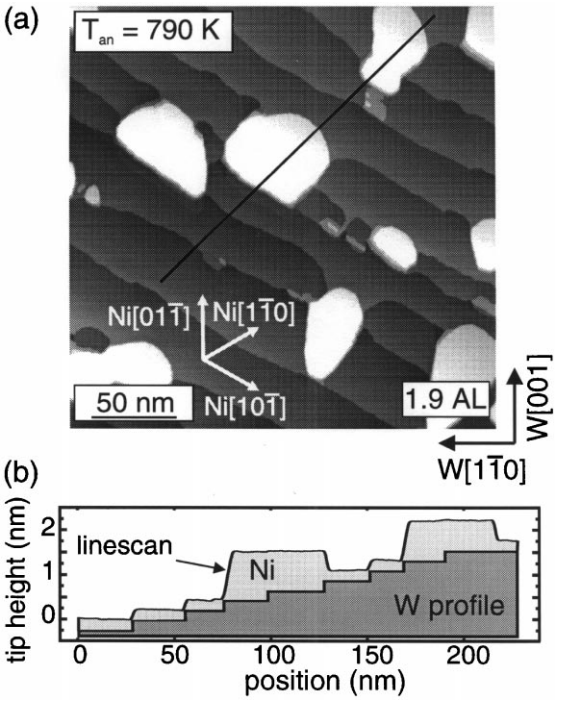

Fig. 5. Influence of annealing on Ni films on W(110). (a) STM image of a film with a total coverage of 1.9 AL, annealed to 790 K. White regions correspond to islands, which have agglomerated upon annealing. The region between the islands is ascribed to a one-atom-thick layer, which is stable for annealing temperatures of up to 900 K, as deduced from annealing films with a thickness of one monolayer. (b) Line scan along the line marked in (a), together with a schematic drawing of substrate steps, denoted the W profile. The islands extend over substrate steps, leading to a locally varying height between 3 and 5 AL.

4. Conclusion

The structural and morphological properties of ultrathin Ni films on W(110) are analysed by STH. While the surprisingly missing preferential orientation of Ni islands below 0.2 ML indicates the diminished importance of strain arguments in this coverage range, the preferential orientation of the second layer islands can be attributed to the anisotropic strain in the completed first atomic layer by taking anisotropic diffusion into account. Starting at coverages of about 5 ML, a preferential orientation of the island edges is observed. The comparison with corresponding systems like Pt/Pt(111) and Al/Al(111) indicates that the observed hexagonally shaped islands are a result of the sixfold in-plane symmetry of the Ni(111) surface.

The analysis of the packing density of the growing film, as obtained from STM images, reveals details of the previously observed structural evolution in the submonolayer range. In an extension of previous LEED work, STM images indicate that the formation of the 8×1 coincidence structure is triggered by coalescence of the islands at a coverage of 0.2 ML. The growth mode of ultrathin Ni films on W(110) at a 300 K change from layer-by-layer to three-dimensional growth at a coverage of about 6 ML. No double-layer growth for coverages below one monolayer was observed. Annealing the films up to 900 K led to the formation of three-dimensional islands on top of a stable first atomic layer, suggesting that the growth of Ni on W(110) in equilibrium proceeds in the Stranski–Krastanov mode.

References

[1] U. Gradmann, in: K.H.J. Buschow (Ed.), Handbook of Magnetic Materials, Vol. 7, Elsevier, Amsterdam, 1993, p. 1.
[2] J.H. van der Merwe, Phil. Mag. A 45 (1982) 127.
[3] D. Sander, C. Schmidthals, A. Enders, J. Kirschner, Phys. Rev. B 57 (1998) 1406.
[4] J.A.C. Bland, B. Heinrich (Eds.), Ultrathin Magnetic Structures, Vols 1 and 2, Springer, Berlin, 1994.
[5] H.J. Elmers, J. Hauschild, H. Höche, U. Gradmann, H. Bethge, D. Heuer, U. Köhler, Phys. Rev. Lett. 73 (1994) 883.
[6] D. Sander, R. Skomski, C. Schmidthals, A. Enders, J. Kirschner, Phys. Rev. Lett. 77 (1996) 2566.
[7] J. Kolaczkiewicz, E. Bauer, Surf. Sci. 144 (1984) 495.
[8] P.J. Berlowitz, D.W. Goodman, Surf. Sci. 187 (1987) 463.
[9] K.P. Kämper, W. Schmitt, G. Güntherodt, H. Kuhlenbeck, Phys. Rev B 38 (1988) 9451.
[10] C. Koziol, G. Lilienkamp, E. Bauer, Appl. Phys. Lett. 51 (1987) 901.
[11] X. Mingde, R.J. Smith, J. Vac. Sci. Technol. A 9 (1991) 1828.
[12] E. Bauer, Appl. Surf. Sci. 11–12 (1982) 479.
[13] C. Schmidthals, D. Sander, A. Enders, J. Kirschner, Surf. Sci. 402–404 (1998) 636.
[14] A.K. Schmid, J. Kirschner, J. Vac. Sci. Technol. B 9 (1991) 649.
[15] U. Scheithauer, G. Meyer, M. Henzler, Surf. Sci. 178 (1986) 441.
[16] D. Sander, A. Enders, C. Schmidthals, J. Kirschner, Surf. Sci. 402–404 (1998) 351.
[17] J.W. Matthews, J.L. Crawford, Thin Solid Films 5 (1970) 187.
[18] J.H. von der Merwe, D.L. Tönsing, P.M. Stoop, Surf. Sci. 312 (1994) 387.
[19] D. Reuter, G. Gerth, J. Kirschner, in: M.C. Tringides (Ed.), Surface Diffusion: Atomistic and Collective Processes, Plenum Press, New York, 1997, pp. 489–498.
[20] K.P. Kämper, W. Schmitt, G. Güntherodt, H. Kuhlenbeck, Phys. Rev. B 38 (1988) 9451.
[21] K.P. Kämper, W. Schmitt, D.A. Wesner, G. Güntherodt, Appl. Phys. A: Solids Surf. 49 (1989) 573.
[22] C. Koziol, G. Lilienkamp, E. Bauer, Phys. Rev. B 41 (1990) 3364.
[23] W.A. Harrison, Solid State Theory, Dover, NY, 1980, p. 94.
[24] J. Fassbender, U. May, B. Schirmer, R.M. Jungblut, B. Hillebrands, G. Güntherodt, Phys. Rev. Lett. 74 (1995) 4476.
[25] H. Bethge, D. Heuer, Ch. Jensen, K. Reshöft, U. Köhler, Surf. Sci. 331–333 (1995) 878.
[26] R.T. Tung, W.R. Graham, Surf. Sci. 97 (1980) 73.
[27] C.-L. Liu, J.B. Adams, Surf. Sci. 265 (1992) 262.
[28] U. Köhler, International Workshop on Determination of Surface Morphology by High Resolution Diffraction, Wohldenberg, Germany, September 1996.
[29] P. Ruggerone, C. Ratsch, M. Scheffler, in: D.A. King, D.P. Woodruff (Eds.), Growth and Properties of Ultrathin Epitaxial Layers, The Chemical Physics of Solid Surfaces, Vol. 8, Elsevier Science, Amsterdam, 1997, pp. 490–544.
[30] T. Michely, M. Hohage, M. Bott, G. Comsa, Phys. Rev. Lett. 70 (1993) 3943.
[31] S. Liu, Z. Zhang, G. Comsa, H. Metiu, Phys. Rev. Lett. 71 (1993) 2967.
[32] R. Stumpf, M. Scheffler, Phys. Rev. Lett. 72 (1994) 254.
[33] Y. Li, K. Baberschke, Phys. Rev. Lett. 68 (1992) 1208.